Fluorescence Correlation Spectroscopy Relates Rafts in Model and Native Membranes

Kirsten Bacia,*† Dag Scherfeld,† Nicoletta Kahya,* and Petra Schwille*†
*Dresden University of Technology, Department of Biophysics, c/o Max-Planck-Institute of Molecular Cell Biology and Genetics, 01307 Dresden, Germany; and †Experimental Biophysics Group, Max-Planck-Institute for Biophysical Chemistry, 37077 Goettingen, Germany

ABSTRACT The lipid raft model has evoked a new perspective on membrane biology. Understanding the structure and dynamics of lipid domains could be a key to many crucial membrane-associated processes in cells. However, one shortcoming in the field is the lack of routinely applicable techniques to measure raft association without perturbation by detergents. We show that both in cell and in domain-exhibiting model membranes, fluorescence correlation spectroscopy (FCS) can easily distinguish a raft marker (cholera toxin B subunit bound to ganglioside (GM1) and a nonraft marker (dialkylcarbocyanine dye dil)) by their decidedly different diffusional mobilities. In contrast, these markers exhibit only slightly different mobilities in a homogeneous artificial membrane. Performing cholesterol depletion with methyl-β-cyclodextrin, which disrupts raft organization, we find an analogous effect of reduced mobility for the nonraft marker in domain-exhibiting artificial membranes and in cell membranes. In contrast, cholesterol depletion has differential effects on the raft marker, cholera toxin B subunit-GM1, rendering it more mobile in artificial domain-exhibiting membranes but leaving it immobile in cell membranes, where cytoskeleton disruption is required to achieve higher mobility. Thus, fluorescence correlation spectroscopy promises to be a valuable tool to elucidate lipid raft associations in native cells and to gain deeper insight into the correspondence between model and natural membranes.

INTRODUCTION

Simons and Ikonen introduced the concept of lipid rafts, in which clusters enriched in cholesterol, sphingolipid, and certain proteins were hypothesized to serve as sorting platforms based on lipid interaction (Simons and Ikonen, 1997; Simons and van Meer, 1988). Such rafts were suggested to give rise to experimentally isolated entities (detergent resistant membranes (DRMs)). This operational raft definition has been applied in a wide range of cell biological studies concerning, e.g., endocytosis, exocytosis, cell signaling, and immunology.

Rafts are thought to result from a distinct lipid phase (liquid-ordered, L_o, as opposed to liquid-disordered, L_d), which is formed in model membranes by long saturated acyl chain lipids together with cholesterol and which is resistant to detergent extraction (Schroeder et al., 1994; Brown and London, 1998). However, DRMs cannot be equated with native rafts, since temperature changes and detergent application can significantly alter phase behavior (Heerklotz, 2002) and since DRMs from different detergents vary in composition (Schuck et al., 2003; Drevot et al., 2002; Braccia et al., 2003). Some markers may associate with or dissociate from rafts, and rafts may coalesce upon detergent treatment (Giocondi et al., 2000). Nevertheless, detergent resistance has become practically the only routine assay for membrane rafts. Since the correspondence between rafts and DRMs and even raft existence are still under debate (Munro, 2003), it is imperative to find new methods that could provide evidence for rafts and raft associations in vivo.

Sensitivity to cholesterol depletion, used as a functional criterion for raft association, can also have undesired effects, since cells may respond to the disruption of lipid compositional balance with structural and metabolic changes. As pointed out by Edidin (2003), actin cytoskeleton may be affected, possibly reducing lateral mobility of membrane proteins. Therefore, a loss of function upon cholesterol depletion cannot pinpoint raft association.

Since native rafts are postulated to be dynamic and fragile structures prone to preparation artifacts, optical methods causing little perturbation provide a promising approach. The high specificity needed for live cell applications is achieved through fluorescent labeling with a small dye or protein (fluorescence resonance energy transfer (FRET), single dye tracing, and fluorescence correlation spectroscopy (FCS)) or through antibody-mediated coupling to a larger bead (photonic force microscopy and single particle tracking). Whereas the risk of labeling artifacts is lower in single dye tracing (Schütz et al., 2000) than in single particle tracking, the disadvantages are lower signal/noise ratios and shorter observable trajectories due to photodamage (Schütz and Hinterdorfer, 2002). It is important to note that none of these methods provides a priori information about structure, but all these methods test predictions derived from a structural model.

In fluorescence correlation spectroscopy, temporal fluorescence fluctuations from the diffusion of single fluorescent molecules through a small, only optically delimited detection volume are monitored (reviewed by Bacia and Schwille, 2003). Excitation and detection are commonly performed

Submitted January 21, 2004, and accepted for publication April 29, 2004.

Address reprint requests to Petra Schwille, Dept. of Biophysics, Dresden University of Technology, Tatzberg 47-51, 01307 Dresden, Germany. Tel.: 49-351-463-40328; Fax: 49-351-463-40342; E-mail: pschwil@gwdg.de.

0006-3495/04/08/1034/10 $2.00

doi: 10.1529/biophysj.104.040519

using a similar laser-illuminated confocal setup as in scanning microscopy. Fluctuations are processed online to yield an autocorrelation curve from which the particle mobility (diffusion coefficient) is derived. FCS works from the single molecule regime up to hundreds of molecules in the focus (from 10-nM to 1-μM concentration range). In contrast to a more elaborate analysis of individual molecule time traces or trajectories (Ha, 2001a,b; Schütz et al., 2000; Schütz and Hinterdorfer, 2002), correlation analysis yields limited insight into the diversity of single molecule behavior. On the other hand, the intrinsic averaging of transition events in FCS provides immediate experimental readout without time-consuming offline analysis and offers high statistical confidence within a short acquisition time. Online readout is especially advantageous for live cell applications, since experimental problems (like a shift of the cell membrane) are easily recognized during data acquisition. Furthermore, in contrast to fluorescence photobleaching recovery/fluorescence recovery after photobleaching (FPR/FRAP) as an instance of a true ensemble method, FCS requires much lower laser powers and only minute, potentially less perturbing fluorophore concentrations.

Although FCS is more commonly applied to three-dimensional probe diffusion, early work already analyzed two-dimensional diffusion in artificial, supported lipid bilayers (Fahey et al., 1977). Later, FCS was applied to native cell membranes (Schwille et al., 1999) and to freestanding artificial lipid bilayers (giant unilamellar vesicles (GUVs)) demonstrating the technique's sensitivity to phase separation (Korlach et al., 1999). We have recently utilized this approach to generate a dynamic phase diagram of the ''canonical lipid raft mixture'' of model membrane studies (unsaturated phosphatidylcholine, cholesterol, and sphingomyelin (SM)) using electroformated GUVs and 1,1′-dioctadecyl-3,3,3′,3′-tetramethylindocarbocyanine perchlorate (diIC$_{18}$) as a marker (Kahya et al., 2003, 2004). GUVs are advantageous, since they can be made truly unilamellar, are not prone to support artifacts, and have sizes and curvatures like the cell plasma membrane.

Despite a great number of FCS studies in recent years, only a few applications have been concerned with membranes, and the technique has not yet been used to study raft phenomena in live cells. Here, we have identified markers for the L_o and L_d phase that are suitable for FCS and have studied their mobilities in GUVs and live cell plasma membranes in a comparative manner. Our results support the existence of rafts in live cells and suggest the use of FCS as a tool to study raft association of membrane constituents in native membranes.

MATERIALS AND METHODS

Chemicals

2-Dioleoyl-*sn*-Glycero-3-phosphocholine (DOPC), *N*-stearoyl-D-erythrosphingosylphosphorylcholine (SM), 1,2-Dilauroyl-*sn*-Glycero-3-phosphocholine (DLPC), and cholesterol were purchased from Avanti Polar Lipids (Alabaster, AL). Monoganglioside-1 (GM1) was from Calbiochem (Merck), (Darmstadt, Germany). Lipids were stored under nitrogen. GUVs were produced either from a 1:1:1 molar mixture of DOPC, SM, and cholesterol (raft mixture) or from pure DOPC, dissolved at 5 mM total concentration in chloroform/methanol (2:1). GM1 was added at 0.1 mol % and the appropriate lipid analog marker at 0.1 mol % for confocal imaging or at 0.001–0.01 mol % for FCS.

Lipid analogs diIC$_{18}$, 1,1′-dihexadecyl-3,3,3′,3′-tetramethylindocarbocyanine perchlorate (diIC$_{16}$), 3,3′-dioctadecyloxacarbocyanine perchlorate (diO), and 1,1′-dioctadecyl-3,3,3′,3′-tetramethylindodicarbocyanine perchlorate (diD), as well as Alexa-488 labeled cholera toxin B subunit (ctxB-488) were obtained from Molecular Probes (Invitrogen), (Carlsbad, CA). For controls, cholera toxin B subunit (from Calbiochem) was labeled with Cy5 monoreactive *N*-hydroxysuccinimide (NHS)-ester (Amersham Biosciences, Piscataway, NJ) and purified on a gel-filtration column (10 DG, Bio-Rad, Hercules, CA). Methyl-β-cyclodextrin (MβCD; Sigma, St. Louis, OH) was dissolved in serum-free minimal essential medium (MEM) for cells or water for GUVs. Cholesterol-recovery complex was prepared as described previously (Pike and Miller, 1998; Klein et al., 1995). A solution of 200 mg MβCD in 2.2 ml water was stirred in an 80°C water bath, and small aliquots of a solution of 6 mg cholesterol in 80 μl isopropanol were added slowly. The resulting clear solution was diluted to 12 mM (with respect to MβCD) in serum-free MEM for cell treatment or water for GUV treatment.

Cell culture

Rat basophilic leukemia cells (RBL)-2H3 and human embryonic kidney (HEK) 293 cells were obtained from the American Type Culture Collection (CRL-2256 and CRL-1573; Rockville, MD). RBL cells were maintained in MEM (Gibco (Invitrogen)), 15% Mycoplex fetal calf serum (PAA Laboratories, Pasching, Austria), nonessential amino acids, 2 mM glutamine, and 1 mM sodium pyruvate (all obtained from Gibco) in a humidified 5% CO_2 incubator at 37°C. HEK cells were cultivated in Dulbecco's modified Eagle's medium (DMEM; Gibco) supplemented with 10% Mycoplex fetal calf serum (PAA Laboratories), 2 mM glutamine, 100 units/ml penicillin, and 100 μg/ml streptomycin (all from Gibco) under the same incubation conditions.

Cell treatments and labeling

Cells were seeded onto 25-mm round coverslips in phenol-red free media and used 24–72 h after plating. Coverslips were mounted in a custom-made chamber at room temperature (22°C) in the media described below. For cholesterol depletion treatment, RBL cells were washed with phosphate-buffered saline (PBS) and placed in the incubator for 20–60 min with 16 mg/ml MβCD in serum-free MEM media. No differences were observed for the different incubation times. For cholesterol recovery complex treatment, previously depleted RBL cells were washed again and incubated for 40–90 min with recovery complex in MEM. To achieve natural cholesterol recovery, previously depleted cells were washed with PBS and incubated with serum-containing media overnight. To disrupt actin cytoskeleton, 5 μM Latrunculin A (Biomol, Plymouth Meeting, PA) was added from a 1000× dimethyl sulfoxid (DMSO) stock to serum-containing media for overnight incubation. For measurements, respective media were supplemented with 10 mM HEPES, pH 7.2, to avoid alkalinization, and with the appropriate concentrations of MβCD, recovery complex, or Latrunculin A to avoid reversal of the treatment. In the case of MβCD and recovery complex supplementation, serum-free media were used. For hypo-osmotic swelling, an equal amount of water was added directly to the measurement media, and swelling was observed under the microscope.

Lipid analog solutions for cell labeling were prepared immediately before use from 1.5-mM lipid analog stocks by ~1000-fold dilution into a 1-mg/ml bovine serum albumin (BSA)/PBS solution, which had been preheated to 37°C. Cells were washed three times with PBS, incubated with lipid analog

for up to 1 min, washed again, and mounted. In the case of MβCD, recovery complex, or Latrunculin A treatments, cells were first treated and then labeled. Lipid analog concentrations and incubation times for labeling were adjusted as needed to obtain the desired intensities for confocal imaging or FCS. CtxB-488 was added in media until the desired degree of labeling was achieved and excess toxin washed away.

Giant unilamellar vesicles

Giant unilamellar vesicles were produced by a modified electroformation method as described previously (Kahya et al., 2003) using a custom-made closed perfusion chamber heated to 65°C and indium-tin-oxide (ITO) coated coverslips as electrodes. Briefly 5 μl lipid mixture was deposited on indium-tin-oxide-coated coverslips. After evaporation of the solvent, the chamber was assembled and filled with 12 mM sucrose solution. A voltage of 1.1 V at 10 Hz was applied. Sucrose solution was employed instead of water to minimize osmotic pressure differences between the interior and the exterior of the GUVs upon addition of MβCD (16 mg/ml, equivalent to 12 mM) or cholesterol recovery complex (same MβCD concentration). Where applicable, ctxB-488 was added to the flow chamber after GUV formation. CtxB-488 was not added for FCS measurements of diI to avoid artifacts from spectral cross talk.

Confocal imaging and FCS

Confocal imaging and FCS measurements were performed on a commercial ConfoCor2 system (Carl Zeiss, Jena, Germany) using standard configurations. Minimal laser powers were chosen to avoid photobleaching (543 nm HeNe Laser: 4 μW; 488 nm Ar-Ion Line: 25 μW and 2.5 μW, achieved by inserting an additional neutral density filter). A 40× NA 1.2 C-Apochromat water immersion objective was used, pinhole sizes set to 90 μm, and pinholes adjusted at least daily. The detection volume was calibrated by measuring the diffusion of a standard dye (tetramethylrhodamine). Calibration was verified by comparing the relation between two- and three-dimensional diffusion (tetramethylrhodamine in water and diI in DLPC GUVs) obtained on the ConfoCor2 and on two different home-built setups. The $1/e^2$ radius of the detection volume for the 543-nm line was determined to be $\omega_o = (0.17 \pm 0.01)$ μm. The dependence of FCS measurements on the accuracy of focus *x-y-z* positioning on the membrane was tested. During measurements, the count rate was monitored. Measurements with a visible drop in count rate that was reversible upon refocusing were excluded to avoid an artifactual bias toward longer diffusion times from shifting membranes. Curves were fitted using a nonlinear least squares algorithm to the model equation commonly used in FCS for two-dimensional, free Brownian diffusion:

$$G(\tau) = N_{\text{eff}}^{-1}\,(1 + \tau/\tau_D)^{-1} + c, \tag{1}$$

where N_{eff} denotes the number of fluorescent molecules in the effective detection volume, c a constant offset due to slow fluorescence fluctuations, and, most importantly, τ_D the diffusion time. In consideration of a blinking phenomenon observed in cyanine dyes, an exponential decay term was also included in the equation (Widengren and Schwille, 2000). In the case of ctxB-GM1 diffusion, an additional diffusion term, weighted with F_{free}, was incorporated to account for a fraction of fast-diffusing, unbound ctxB. $\tau_{\text{diff,free}}$ was determined in a separate measurement.

$$G(\tau) = N_{\text{eff}}^{-1}(F_{\text{free}}(1 + \tau/\tau_{\text{diff,free}})^{-1} + (1 - F_{\text{free}})(1 + \tau/\tau_D)^{-1}) + c. \tag{2}$$

Diffusion coefficients in Table 1 were evaluated according to $D = \omega_o^2/(4\tau_D)$. To facilitate the comparison between GUVs and native membranes, the same model was used for all diI curves. However, curves obtained on native membranes are better described as slightly anomalous (Schwille et al., 1999). Standard deviations of τ_D were calculated from measurements compromising upper and lower membranes of multiple GUVs or cells. Errors may also be estimated from the inspection of single measurements displayed in Fig. 2.

TABLE 1 Probe mobilities in GUVs and cell plasma membranes

Fig.	Marker	System	Treatment*	Domain	$\tau_D \times$ ms	$D \times$ cm^2/s
2 *E*	$diIC_{18}$	DOPC GUVs	–	Homogeneous (L_d)	1.03 ± 0.05	(7.0 ± 1.2) × 10^{-8}
2 *E*	$diOC_{18}$	DOPC GUVs	–	Homogeneous (L_d)	0.8 ± 0.1	(7.0 ± 1.2) × 10^{-8}
2 *E*	ctxB-488 GM1	DOPC GUVs	–	Homogeneous (L_d)	1.5 ± 0.2	(3.6 ± 1.4) × 10^{-8}
2 *A*	$diIC_{18}$	Raftmix GUVs	–	Bright-red (L_d)	1.51 ± 0.09	(4.8 ± 0.9) × 10^{-8}
2 *A*	$diIC_{18}$	Raftmix GUVs	MβCD	Homogeneous (L_d)	3.7 ± 0.6	(2.0 ± 1.0) × 10^{-8}
2 *F*	ctxB-488 GM1	Raftmix GUVs	–	Bright-green (L_o)	12.0 ± 0.6	(4.5 ± 1.4) × 10^{-9}
2 *F*	ctxB-488 GM1	Raftmix GUVs	MβCD	Homogeneous (L_d)	3.2 ± 1.0	(1.7 ± 1.0) × 10^{-8}
2 *B*	$diIC_{18}$	RBL	–	Nonraft?	8.7 ± 0.8	(8.3 ± 1.7) × 10^{-9}
2 *B*	$diIC_{18}$	RBL	MβCD	Nonraft?	18.7 ± 1.5	(3.9 ± 0.8) × 10^{-9}
2 *B*	$diIC_{18}$	RBL	1. MβCD, 2. Chol.	Nonraft?	12.4 ± 3.0	(5.8 ± 2.1) × 10^{-9}
2 *C*	$diIC_{18}$	HEK 293	–	Nonraft?	5.0 ± 0.5	(1.4 ± 0.3) × 10^{-8}
2 *C*	$diIC_{18}$	HEK 293	MβCD	Nonraft?	7.9 ± 0.9	(9.2 ± 2.2) × 10^{-9}
2 *D*	$diIC_{16}$	RBL	–	Nonraft?	8.1 ± 0.9	(8.9 ± 2.1) × 10^{-9}
2 *D*	$diIC_{16}$	RBL	Different day	Nonraft?	8.2 ± 1.6	(8.8 ± 2.8) × 10^{-9}
2 *D*	$diIC_{16}$	RBL	MβCD	Nonraft?	12.1 ± 2.1	(6.0 ± 1.8) × 10^{-9}
2 *D*	$diIC_{16}$	RBL	1. MβCD, 2. serum	Nonraft?	7.5 ± 1.6	(9.6 ± 3.2) × 10^{-9}
2 *D*	$diIC_{16}$	RBL	Hypo-osmotic	Nonraft?	7.8 ± 1.2	(9.3 ± 2.5) × 10^{-9}
3 *C*	ctxB-488 GM1	RBL	–	Raft?	Immobile	Immobile
3 *C*	ctxB-488 GM1	RBL	MβCD	Raft?	Immobile	Immobile
3 *C*	ctxB-488 GM1	RBL	Latr. A	Raft?	≈60	≈1 × 10^{-9}

*Methyl-β-cyclodextrin (MβCD) reduces membrane cholesterol; soluble, MβCD-complexed cholesterol (Chol.) increases membrane cholesterol; and Latrunculin A (Latr. A) disrupts actin cytoskeleton.

RESULTS

In situ change of cholesterol content in GUVs

GUVs were prepared from a ternary lipid mixture of DOPC/SM/cholesterol = 1:1:1 plus 0.1% GM1 (raft mixture). These vesicles exhibit an L_d-L_o phase separation (Dietrich et al., 2001), which can be visualized by fluorescent markers (Fig. 1 *A*).

As we have recently shown by FCS analysis of $diIC_{18}$ mobility (Kahya et al., 2003), the red marker becomes enriched in the less ordered (L_d) phase ($D = 5 \times 10^{-8}$ cm^2/s) and is present at low concentration in the more ordered L_o domains ($D = 0.8 \times 10^{-8}$ cm^2/s, i.e., ≈sixfold slower). This was rather unexpected, since in the case of the coexistence of L_d and gel phase, the long-chain diIs, such as $diIC_{18}$, prefer the more ordered (i.e., the gel) state (Klausner and Wolf, 1980; Spink et al., 1990). Our conclusion that $diIC_{18}$ preferentially labels the L_d phase is confirmed through counterstaining of the L_o phase by binding Alexa-488 labeled cholera toxin B subunit to the ganglioside GM1 (Fig. 1 *A*). Analogous results are obtained (data not shown) if $diIC_{18}$ is substituted by $diIC_{16}$, by diO (C_{18} carbon chain, green fluorescence), or by diD (C_{18}, far red fluorescence), and if Alexa-488 labeled cholera toxin B subunit is substituted by Cy5 labeled cholera toxin B subunit (far red fluorescence).

Cholesterol depletion from membranes by the addition of MβCD, an important tool in cell biological raft studies, is expected to suppress L_o phase formation. Here we observe the effect of MβCD on GUVs from a simple ternary lipid mixture in situ by confocal laser scanning. With MβCD addition, the clearly visible domain separation (Fig. 1 *B*) disappears, starting under our experimental conditions at the phase borders (Fig. 1 *F*), and leaves behind GUVs that appear uniformly labeled with both probes on the scale of optical resolution (Fig. 1 *C*).

This process is reversible. Phase separation is restored when a cholesterol-loaded MβCD complex is added to previously cholesterol-depleted GUVs (Fig. 1, *D* and *E*). Many small domains emerge that apparently increase in size and fuse to give rise to large domains (Fig. 1 *G*).

FCS is sensitive to phase and composition dependent viscosity

The diffusion time τ_D is a measure of the average time it takes the fluorescent marker to move through the focus. τ_D is easily derived from the FCS curves as the half-value decay time (or more accurately obtained from the numerical fits) and allows for precise calculation of the diffusion coefficient D. All diffusion times and diffusion coefficients obtained from numerical fitting are summarized in Table 1.

The diffusion properties of the marker diI, indicated by the red curves in Fig. 2 *A*, reflect the mobility of this marker in raft mixture GUVs in the brightly labeled L_d phase ($\tau_d = 1.5$ ms). As the domains are dissolved by in situ cholesterol depletion, diffusion slows down to $\tau_D = 3.7$ ms in the resulting uniform phase.

The same qualitative effect is observed for the far more complex system of live cell plasma membranes. Fig. 2 *B* compares the diffusion of a $diIC_{18}$ marker in the plasma membrane of untreated RBL cells (*red curves*) with $diIC_{18}$ on cells treated with MβCD. Analogous to the simple artificial system, diI diffusion is slower after cholesterol depletion. Fig. 2 *C* shows the results from the same experiment performed on a different cell line (HEK 293). Again, the diffusion of the presumable nonraft marker is slowed down when rafts are supposedly broken up by

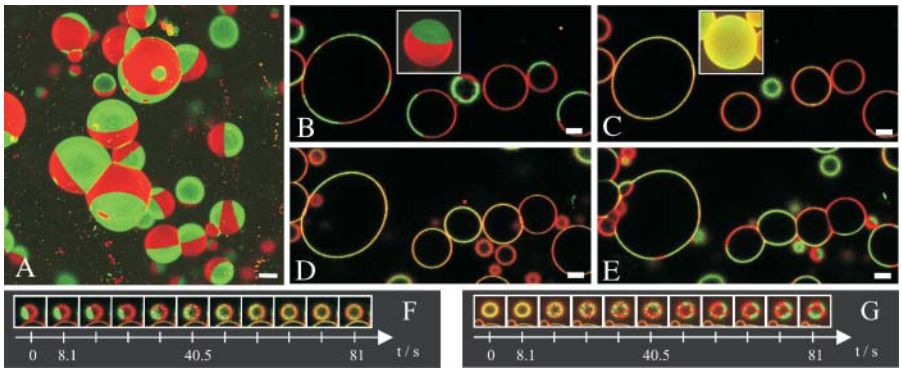

FIGURE 1 GUVs exhibit phase separation into L_d (*red*) and L_o (*green*) domains that is reversibly removed by in situ cholesterol extraction. All scale bars = 10 μm. Fig. 1 *A* shows a three-dimensional reconstruction of giant unilamellar vesicles from confocal slices. GUVs were prepared from DOPC/SM/cholesterol = 1:1:1 with the addition of $diIC_{18}$ and GM1 in trace amounts. CtxB-488, which binds to GM1, has been added after the preparation. $DiIC_{18}$ fluorescence is depicted in red and ctxB-488 fluorescence in green. As the vesicles, which were produced above the melting temperature of the lipid mixture, approach room temperature, domains grow large. Spherical domain borders confirm the coexistence of two liquid phases (L_o and L_d). Fig. 1, *B* and *C*, represents confocal slice images (*insets*: three-dimensional reconstructions) of GUVs prepared from the same composition, before and after addition of MβCD, a cholesterol-sequestering agent. Cholesterol depletion results in GUVs that are uniformly labeled with both probes (*red*: diI; *green*: GM1-ctxB-488; and *yellow*: overlay). The slightly stronger red fluorescence on the right and left sides of GUVs in the confocal sections (Fig. 1, *B–E*) is due to the polarization of the laser light and the orientations of the diI chromophores in the membrane. It does not indicate an uneven distribution of diI in Fig. 1, *C* and *D*. During the time course of cholesterol depletion (Fig. 1 *F*), dissolution appears to be initiated at the borderline between domains. The ''lifesaver''-like appearance of this GUV (diameter ≈ 10 μm) stems from the confocal imaging of a slice below the top of the vesicle. Previously depleted GUVs (Fig. 1 *D*) are treated with cholesterol-loaded MβCD complex, resulting in a reappearance of domains (Fig. 1 *E*). Smaller domains emerge first and then coalesce (Fig. 1 *G*; GUV diameter ≈ 15 μm). The tendency of whole GUVs to attach to each other and fuse is probably due to osmotic effects or changes in lipid molecule numbers in the membrane.

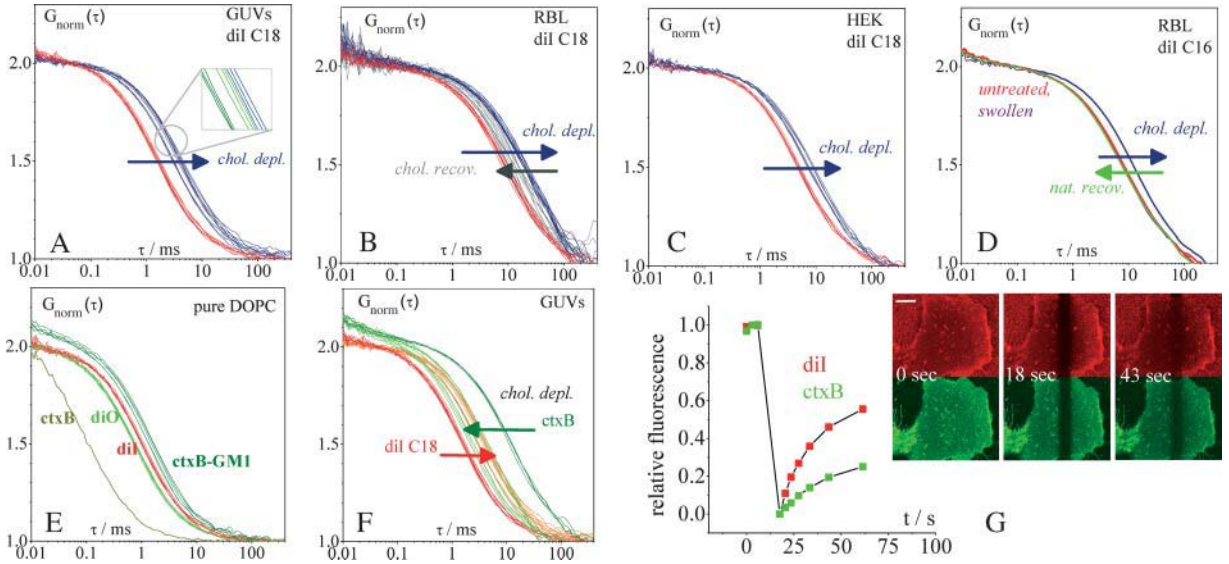

FIGURE 2 In situ cholesterol depletion reduces the mobility of the nonraft marker diI both in GUVs and in native membranes. The red curves in Fig. 2 *A* represent diIC$_{18}$ diffusion in the bright phase of raft mixture GUVs. After in situ cholesterol depletion, diffusion in the resulting homogeneous phase is slower (*blue curves*; see also summary of all data in Table 1). The blow-up displays curves taken on the same vesicle in a distinct color: Even the slight differences in mobility between single vesicles due to variations in lipid composition are detected demonstrating the high sensitivity achievable by FCS analysis. Fig. 2 *B* show the diffusion of the same marker, diIC$_{18}$, measured on live RBL cell plasma membranes (*red curves*). Absolute marker mobility is distinct from the one observed in GUVs. When cholesterol is depleted by MβCD treatment, marker diffusion becomes slower. The addition of complexed cholesterol to previously depleted cells causes diI to become more mobile again, but mobility is still lower than in cells with natural cholesterol content. Fig. 2 *C* depicts the cholesterol depletion experiment performed on a different cell line (*HEK* 293). Again, diIC$_{18}$ diffusion is slower after cholesterol depletion, which agrees with the findings on the RBL cells. Fig. 2 *D* shows the effect of cholesterol depletion on the diffusion of diIC$_{16}$ in RBL cell plasma membranes (both *red lines*: untreated cells; *blue line*: MβCD treated cells). This experiment demonstrates that diIC$_{16}$, which was assumed to be a raft marker by Hao et al. (2001), behaves qualitatively the same as diIC$_{18}$. Fig. 2 *D* also contains three more control experiments. For clarity, only average curves are depicted. 1), Mobility for a given cell line is very reproducible, as the averages of two sets of measurements recorded on two different days (*red lines*) show. 2), DiI marker mobility in previously cholesterol depleted cells was found to be completely restored when cells were allowed to recover naturally in serum-supplemented media (*green line*). 3), Hypo-osmotic swelling (*gray line*) had no significant effect on diI mobility in comparison with untreated cells. Fig. 2 *E* demonstrates that the diffusion of ctxB-488 that binds to a maximum of five GM1 molecules is only twofold slower in a homogeneous artificial membrane (*DOPC*) than the diffusion of diIC$_{18}$ or diOC$_{18}$. (See also summary of all data in Table 1.) The markers diIC$_{18}$ and diOC$_{18}$, which are structurally similar but have different fluorescent spectra, are assumed to possess the same mobility ($D = 7 \times 10^{-8}$ cm^2/s). However, diI is observed to bear a longer diffusion time (*red lines*) than diO (*left green lines*), which is due to the wavelength dependence of the focal area. Therefore, when comparing ctxB-GM1 mobility to diI mobility in FCS curves by eye, the relation of diI and diO curves needs to be borne in mind. This complication does not arise in the comparison of diffusion coefficients, where the calibration of the detection volume has already been accounted for (Table 1). To allow direct visual comparison of diffusion decays in the case of membrane-bound ctxB, where an additional contribution of unbound ctxB is observed in the curves, normalization has been carried out with respect to the slow-diffusing component. The contributions were quantitated using a two-component fit, in which the diffusion time of the fast component was known from a separate measurement (*gray line*: $\tau_D = 110$ μs and $D = 5.0 \times 10^{-7}$ cm^2/s). The relative amplitude of free ctxB, which appears as a shoulder in the ctxB-curves at shorter times, depends on the concentration of ctxB added to the GUVs in the particular experiment. It was $F_{free} = (7.9 \pm 1.1)\%$ in Fig. 2 *E* and $F_{free} = (9.6 \pm 0.8)\%$ in Fig. 2 *F*. Fig. 2 *F* shows that ctxB-GM1 has a considerably lower mobility in the L_o domains of raft mixture GUVs (*dark green curves*) than in the homogeneous DOPC membrane (Fig. 2 *E*). When domain separation is abolished by cholesterol depletion, mobility greatly increases (*bright green curves*). For comparison, the FCS curves showing the decrease in mobility of diI in its phase of enrichment (L_d, *red curves*) versus the homogeneous phase after depletion (*orange curves*) are shown again, the same as in Fig. 2 *A*. Fig. 2 *G* shows a FRAP experiment performed on the bottom membrane of an HEK 293 cell, double-labeled with diIC$_{18}$ and ctxB-488. Both markers were bleached simultaneously in a rectangular area. The recovery of diI is obviously faster than that of ctxB-488 as seen in the representative images and in the fluorescence quantitation from the bleached region of interest (fluorescence was set relative to a control region, bleach depth was scaled to 100%, and the scale bar =10 μm).

cholesterol depletion. However, absolute mobilities differ between GUVs and cells and also between the different cell lines. The mobilities are reproducible within each cell line and for the GUVs. (See for instance the *two superimposing red curves* in Fig. 2 *D* that represent average diIC$_{16}$ mobility in RBL cells recorded on different days.) Their dependency on cell type can be explained by cell-type specific membrane lipid composition. The analogy in the mobility shift seen in GUVs, HEK, and RBL cells indicates that cholesterol depletion plays a unique role, inducing the same qualitative effect in all investigated systems.

To test for the reversibility of cholesterol depletion, cholesterol-recovery complex was added to previously depleted cells. This treatment succeeded to partially restore diI mobility in the cell membrane (Fig. 2 *B*). However, presumed raft disintegration was completely reversible when cells were allowed to recover from depletion in media supplemented with serum (*natural recovery*, Fig. 2 *D*).

Furthermore, the marker diIC$_{16}$, which was used by Hao et al. (2001), shows the same qualitative behavior upon depletion as diIC$_{18}$ (Fig. 2 *D*). Since cholesterol depletion by MβCD is observed to change cell morphology toward more rounded cells (compare Fig. 3, *A* and *B*, *middle columns*), it was also tested whether the observed diffusion is sensitive to membrane topology. Although surface deformations appear more pronounced on upper than on lower membranes (compare Fig. 3 *A*, *right* and *left columns*), no mobility differences were found between diI measurements carried out on upper and lower cell membranes. (All data includes measurements on both sides of the cells; distinction is not marked.) Furthermore, since cholesterol depletion appeared to somewhat reduce surface deformations, hypo-osmotic swelling was performed but was found to have no significant effect (Fig. 2 *D*).

Cholera toxin B subunit bound to GM1 in the L_o domain is far less mobile than dil in the L_d domain

Before interpreting the original FCS data and diffusion times (τ_D) of ctxB-488 and diI, it is important to recall the wavelength dependence of the size of the focal area. For instance, diI (*red*) and diO (*green*, spectrally similar to ctxB-488) should have the same diffusion coefficients, but the red marker shows a longer diffusion time than the green marker (Fig. 2 *E* and Table 1).

The diffusion of GM1-bound ctxB-488 in a homogeneous DOPC GUV membrane is only ~twofold slower than that of diI (Fig. 2 *E* and Table 1). However, in raft mixture GUVs, GM1-bound ctxB-488 diffuses about one order of magnitude (≈11-fold) slower in its preferred phase than diI in its respective phase of enrichment (Fig. 2 *F*). If phase separation is reversed by cholesterol depletion, ctxB-488 GM1 and diI exhibit similar diffusion behavior (Fig. 2 *F*), with some variations among GUVs.

Phase domains are clearly distinguishable in GUVs allowing FCS measurements to be carried out in only one domain (either diI-enriched or ctxB-GM1 enriched), whereas no complementary staining on a microscopically visible scale is observed in native membranes (Fig. 3 *A*). On the contrary, colocalized staining patterns of diI and ctxB-488 are observed on the upper membrane of RBL cells (Fig. 3 *A*, *right column*). This imaging result is misleading. The effect most likely results from surface topology and must not be interpreted as a colocalization of the two markers in rafts, since the mobility of ctxB-GM1 (*green*) and diI (*red*) are actually extremely different from each other. Whereas diI mobility is well accessible by FCS (Fig. 2 *B*), cholera toxin diffusion is so slow that it is photobleached on its way through the focus, which corrupts the autocorrelation curve (Fig. 3 *C*, *upper graphs*). This observation of the very different mobilities of diI and ctxB is confirmed by FRAP on double-labeled HEK cells (Fig. 2 *G*). Clearly, diI recovers

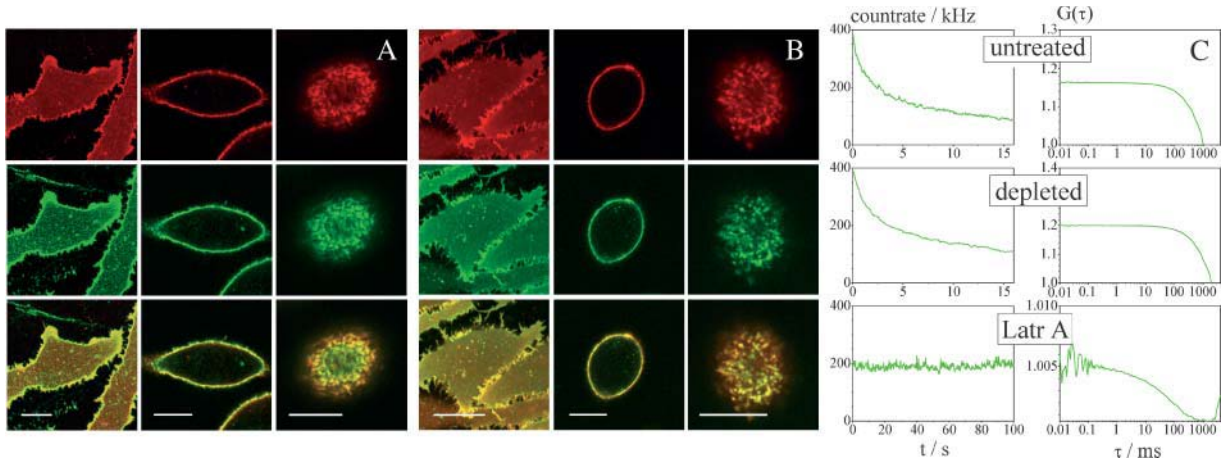

FIGURE 3 Confocal scanning microscopy does not show phase separation in native cell membranes; FCS reveals low, cytoskeleton-dependent mobility of cholera toxin in native membranes. (*A*) Images of a live RBL cell immediately after double labeling with diIC$_{18}$ (*red*) and ctxB-488 (*green*) in the native cholesterol state were taken at the bottom membrane near the coverslip (*left column*), at the equatorial plane (*middle column*), and at the top membrane (*right column*). Scale bar = 10 μm. The same kind of confocal sections were obtained of a cell in the cholesterol-depleted state (*B*). Evidently, diI and ctxB do not become enriched in microscopically visible, counterstained domains, as seen from the overlays in the bottom rows of *A* and *B*. However, at the upper side of the cell (*right bottom images*), there is colocalized staining, probably arising from membrane topology. Note that cell morphology changes upon cholesterol depletion (*middle columns*). Similarly, cells became more rounded under conditions of hypo-osmotic swelling (not shown). The upper left graph in Fig. 3 *C* shows the fluorescence count-rate trace of an attempted FCS measurement on the membrane of an RBL cell. There is strong photobleaching even at low laser powers, confirming very low ctxB-GM1 mobility ($\tau_D > 70$ ms and $D < 1 \times 10^{-9}$ cm^2/s). The loss in fluorescence leads to an artifactual decay in the correlation curve (*upper right graph*) that cannot be interpreted by standard FCS models. The middle graphs of *C* depict a representative attempt to measure the mobility of ctxB on an RBL cell after cholesterol depletion with MβCD. Despite this treatment, which is assumed to disrupt raft integrity, the low mobility of ctxB-GM1 clearly remains. In contrast, when actin cytoskeleton was disrupted by Latrunculin A treatment, ctxB-GM1 tended to be more mobile: The bottom graphs in *C* show a count rate that does not decay and an FCS curve that is not corrupted by bleaching.

faster than ctxB-488. Unfortunately, this type of area-bleach FRAP experiment is experimentally difficult to control due to cellular movements and endocytosis during longer recovery acquisition times.

Since FCS depends on the mobility of molecules, in the case of low mobility of raft components, photobleaching arises that corrupts the autocorrelation curves (Fig. 3 *C*, *upper graphs*). Also, an apparent mobile fraction remaining after bleaching can be an artifact generated by ctxB that has already been endocytosed into small vesicles (Bacia et al., 2002). Further reduction of laser power was impracticable, since it diminished the signal (particle brightness) to such extent that correlation curves could no longer be obtained. It is noteworthy though that ctxB mobility is even slower than expected from the experiments on domain-exhibiting GUVs. If the diffusion time of ctxB in the native membrane was by the same factor slower than that of diI as in GUVs, it would be in the range of 40 ms (HEK) or 70 ms (RBL). In this case, we would still expect it to be accessible by FCS at low laser powers and with the highly efficient setup used here, but this was generally not the case. Curiously however, ctxB often did fall into the mobility range accessible by FCS when it was measured on rounded, dividing cells or on membrane patches, produced by sonication (Avery et al., 2000) before ctxB labeling (data not shown). Since these observations point to a role of the actin cytoskeleton in GM1 or raft mobility, cells were treated overnight with Latrunculin A. This kind of actin cytoskeleton disruption was able to render ctxB quite mobile and accessible by FCS (Fig. 3 *C*, *bottom*). The fluorescence count rate after Latrunculin A treatment was usually more stable, and the correlation curve obtained a result from true ctxB diffusion and not a bleaching artifact. These observations jointly point to a role of actin cytoskeleton in GM1 or raft mobility. In contrast, cholesterol depletion with MβCD did not render ctxB-488 mobile on native membranes, as indicated by photobleaching (Fig. 3 *C*, *middle*).

DISCUSSION

FCS analysis of domain-exhibiting GUVs

By confocal imaging and FCS, enrichment and diffusional mobilities of two fluorescent markers (diI and ctxB-488-GM1) were analyzed in a GUV model membrane system. The probes have opposite phase preference and are well suited for FCS. In raft mixture GUVs, ctxB-GM1 is an L_o (raft) phase marker and diI an L_d (nonraft) phase marker. The markers exhibit a large (11-fold) diffusional mobility difference in their respective phases, whereas there is only a small (twofold) difference between their mobilities when they are located in the single phase of homogeneous DOPC GUVs. Thus, the restrictive effect of lipid order (L_o phase) on the diffusion coefficient is much larger than the effect of the size of the ctxB-GM1 complex versus the diI molecule. As evident from the images, the large L_o and L_d domains in raft mixture GUVs allow for the FCS focus to be positioned within such a domain. From FCS measurements, there is no indication for an extra, *subresolution micro*domain structure within these visible domains, since FCS curves on GUVs fit well to a normal diffusion model.

Effect of MβCD on L_o domains

Our dynamic phase diagram for the raft mixture lipids in GUVs (Kahya et al., 2003) predicts a loss of phase separation, a decrease of the L_d phase marker mobility, and an increase of the L_o marker mobility, if enough cholesterol is extracted. We found that cholesterol depletion by MβCD, a reagent that is commonly used on native membranes with the purpose of disrupting rafts, abolishes the L_o domains in GUVs and produces the predicted effects on diffusional mobilities.

FCS analysis on cell membranes

Judging from the high mobility of diI in contrast to ctxB in cell membranes, diI shows the same partitioning as in the artificial membranes, i.e., enrichment in the nonraft phase, and diI diffusion takes place in a phase that is continuous over the dimensions of the focus. Nevertheless, *subresolution* rafts that are poor in diI may act as obstacles to diI diffusion in the nonraft phase and lead to shallow FCS decays, describable by an anomalous diffusion model (Saxton, 1994). Indeed, the shape of diI FCS curves in native membranes is better described by introducing the anomaly parameter ($\alpha = 0.8$ for RBL; compare with Schwille et al., 1999), supporting a subresolution structure of small rafts dispersed in a continuous, diI-enriched nonraft phase.

For the raft-marker ctxB-488, there should be no resolvable fluorescence fluctuations from diffusion within rafts that are smaller than the focus, and the marker will be bleached if it is unable to leave the focus (Fig. 3 *C*, *upper* and *middle*). The extremely low mobility observed for ctxB-GM1 in comparison with diI therefore suggests its restriction to structures like rafts or cross-linked raft assemblies. The susceptibility of ctxB mobility to actin cytoskeleton disruption (Fig. 3 *C*, *bottom*) supports that these rafts are associated with cytoskeleton, which is in agreement with previously reported evidence (Seveau et al., 2001; Caroni, 2001; Yoon et al., 2003). As the lipid moiety of GM1 cannot directly interact with the cytoskeleton (Craig and Cuatrecasas, 1975), the association with other lipids and/or proteins in rafts provides an explanation for the observed cytoskeleton dependence. Since cholera toxin greatly increases the detergent resistance of GM1 (Hagmann and Fishman, 1982), it will now be of interest to investigate the mobilities of membrane proteins that are raft and nonraft markers according to their DRM associations, to be able to further discriminate the roles of raft

association and raft cross-linking and to test the DRM hypothesis.

If no bleaching occurs and an FCS curve as in the bottom of Fig. 3 *C* is obtained, this may be due to either association-dissociation kinetics of ctxB-488 to and from the raft or to movement of the whole raft through the focus, where the latter is more likely to be dominant, as mobility is modulated by actin cytoskeleton disruption. We do not attempt to calculate a raft diameter from the diffusion coefficient (Pralle et al., 2000), since it remains unclear if there is still impairment of raft mobility on the measurement scale. Nevertheless, the observation of rafts diffusing through the focus would open up the possibility of analyzing raft marker colocalization using a dynamic dual-color cross correlation approach as demonstrated for endocytic vesicles (Bacia et al., 2002). This technique could prove superior to scanning or image cross correlation, since static techniques inevitably pick up correlated brightness patterns due to morphology (Fig. 3, *A* and *B*).

Effect of MβCD on native rafts

In the GUV model system, MβCD subverts the L_o state, assimilating nonraft (diI) and raft-marker (ctxB-GM1) mobilities. Using the common procedure of MβCD application to native membranes to disrupt rafts, we find in analogy to the GUVs that diI mobility is decreased. Given that in the coexistence regime of ternary raft mixture GUVs, diI mobility in the L_d phase is virtually independent of cholesterol concentration (Kahya et al., 2003) and in a binary DOPC/cholesterol mixture, diI mobility increases with decreasing cholesterol concentration (Kahya et al., 2004), cholesterol-rich rafts provide a good explanation for the decrease in diI mobility observed upon MβCD application. Thus the effect of MβCD seen on diI mobility supports that native rafts exist and are at least partially destructed by cholesterol depletion. However, surprisingly, the raft marker ctxB is not rendered mobile (Fig. 3 *C*, *middle*) by MβCD application. Possibly, cholesterol depletion starts at the more vulnerable boundary zones, leaving behind core rafts that remain cytoskeleton attached and still contain strong raft markers, like GM1-ctxB. Interestingly, Schuck et al. (2003) reported that MβCD treatment on intact MDCK cells did not reduce DRM association, but only MβCD treatment on already homogenized cells effectively displaced raft marker proteins from the DRM to the soluble fraction. Again, this indicates the involvement of cellular structures in ensuring raft stability that are susceptible to homogenization, like cytoskeleton association or membrane morphology and undoubtedly raises questions about how MβCD really affects rafts when used in functional raft studies on live cells.

The partial reversal of diI mobility observed upon application of the cholesterol recovery complex may be due to excessive cholesterol restoration or cellular changes in response to MβCD. Oversaturation with cholesterol has been seen to slow down diI mobility and remove phase separation in raft mixture GUVs (Kahya et al., 2003). In contrast, when cells recover naturally, reduction in diI mobility is completely reversible.

Selection of fluorescent probes

In contrast to the exclusive use of diI in our previous GUV studies, two markers with opposite phase preference were required in the case of native cells. The rationale is that in GUVs domains are on the order of several micrometers, and the focus is easily positioned within a domain, but in cells with submicron domains both phases are simultaneously present in the focus, and only the enriched marker contributes to the fluorescence signal.

Even long-chain dils act as nonraft markers

Despite their preference for the more ordered phase in gel-L_d coexistence, we find both in artificial and in native membranes that long-chain diIs (diC_{16} and diC_{18}) prefer the less ordered phase in the L_o-L_d coexistence, contradicting earlier assumptions (Hao et al., 2001). DiI in our experiments was always completely mobile as shown, it never reached the 10^{-10} cm^2/s or bleaching regime typical of gel phase. Thus there appears to be no extended gel phase in the native, unperturbed membrane. Along this line, it seems conceivable that the colocalization of diI with raft-derived patches of FcεRI (Thomas et al., 1994) after cross-linking for 2 h at 4°C was due to the formation of gel phase domains under these nonphysiological conditions.

Advantages of fluorescence correlation spectroscopy

This study demonstrates that FCS accurately and reproducibly determines even small differences in lateral mobility in live cell membranes within short acquisition times and using a commercially available setup. FCS may thus prove useful for investigating raft phenomena in native membranes, offering the following advantages over FRAP. First, the small fluorophore concentration used in FCS is biochemically less perturbing than the strong labeling used in FRAP. Second, in the spot bleaching variant of FRAP, a short, very strong bleach pulse with a laser intensity on the order of 100-fold higher than in our FCS measurements is needed. In combination with the higher fluorophore concentration, this makes serious heating artifacts much more likely than in FCS (compare with the calculation by Axelrod, 1977). Other FRAP protocols employ lower laser power but large bleach regions and long recovery times, making them sensitive to interference from live cell movements. Long observation times (longer than in Fig. 2 *G*) are however necessary to derive meaningful diffusion coefficients in the case of

multiple recovery kinetics or at least to quantitate a so-called immobile fraction. In contrast, due to the short acquisition time, FCS is less susceptible to movements, and the occurrence of such artifacts is easier to recognize, since the count rate in unperturbed FCS measurements is constant on long timescales. Third, signal/noise decreases in FRAP due to continuous bleaching, and finally, depending on the geometry, special mathematical modeling may be needed to fit the photobleaching recovery curve (Siggia et al., 2000).

The limitation of FCS lies in determining diffusion coefficients of slowly moving membrane components. To quantitatively assess the mobility of, e.g., ctxB-GM1 in native membranes, the dynamic range of FCS will need to be extended, either by devising setups with smaller detection volumes or by designing novel, more stable fluorescent markers.

Complexity of native membranes in comparison to the model system

Despite the analogy observed in this study, membrane structure in cells is by far not as simple as the L_d and L_o phase separation in the artificial system. Possible complications include associations in membranes that are not extended enough to be called phases (that might be better viewed as cholesterol complexes; McConnell and Vrljic, 2003, review), effects of border regions between phases, and consequences of asymmetric lipid distributions. In addition, live cell membranes are not in thermodynamic equilibrium, but some associations are regulated by directed, energy-consuming processes. Also, the complex lipid composition causes a broad thermal transition with the physiological temperature falling into this range (Yeagle, 1991), which may be the reason for the small size of the postulated in vivo domains (Marsh et al., 1976). A similar effect could be exerted by proteins acting as impurities in real membranes. Furthermore, there might be an interplay between membrane curvatures and domain size (Marsh et al., 1977). We have observed a morphological tolerance at the phase borders in GUVs (data not shown), as seen by Baumgart et al. (2003). Conversely, morphology imposed by the cytoskeleton could limit favorable domain size in native membranes.

The role of temperature

In a eukaryotic cell, a broad thermal transition has the advantage that cellular functions are only gradually reduced in a low temperature environment. For example, membrane internalization still occurred at room temperature but at a much slower rate than at 37°C. We preferred working at room temperature due to significant experimental advantages. We have observed a loss in FCS signal (molecular brightness) at higher temperatures, and internalized diI starts to perturb the measurements much sooner. Nevertheless, investigations of marker mobilities at different temperatures would be of interest. Under different experimental conditions (different cell type and different depletion method) and using a different technique (FRAP), Thompson and Axelrod (1980) found that diI mobilities in nondepleted and depleted membranes became more similar with increasing ambient temperature. However, they used a 100-fold stronger laser intensity that may have critically elevated local temperature (see discussion by Axelrod, 1977).

To summarize, we have shown that fluorescence correlation data on membranes can be obtained with a very good signal and excellent reproducibility, allowing analysis of marker mobility in live cell membranes. We have taken advantage of the applicability of FCS to both artificial and natural membranes for comparative analysis. The observation of both similarities and differences gives insight into the qualities of artificial membranes as a model for native cell membrane organization. FCS is demonstrated to be a promising technique for distinguishing raft-associated and nonraft membrane components based on lateral mobility under natural conditions, without the use of detergents.

We thank Kai Simons and Sebastian Schuck, other interested scientists, and group members for discussions and comments. Karin Birkenfeld assisted with cell culture. Sally Kim is acknowledged for useful discussions and help with this manuscript. The study was carried out in collaboration with Carl Zeiss, Jena.

Financial support was provided by the Volkswagen Foundation and the German Ministry of Education and Research (grants 0311845 and 16SV1257).

REFERENCES

Avery, J., D. J. Ellis, T. Lang, P. Holyroyd, D. Riedel, R. M. Henderson, J. M. Edwardson, and R. Jahn. 2000. A cell-free system for regulated exocytosis in PC12 cells. *J. Cell Biol.* 148:317–324.

Axelrod, D. 1977. Cell surface heating during fluorescence photobleaching recovery experiments. *Biophys. J.* 18:130–131.

Bacia, K., I. V. Majoul, and P. Schwille. 2002. Probing the endocytic pathway in live cells using dual-color fluorescence cross-correlation analysis. *Biophys. J.* 83:1184–1193.

Bacia, K., and P. Schwille. 2003. A dynamic view of cellular processes by in vivo fluorescence auto- and cross-correlation spectroscopy. *Methods.* 29:74–85.

Braccia, A., M. Villani, L. Immerdahl, L. L. Niels-Christiansen, B. T. Nystrom, G. H. Hansen, and E. M. Danielsen. 2003. Microvillar membrane microdomains exist at physiological temperature. Role of galectin-4 as lipid raft stabilizer revealed by ''superrafts''. *J. Biol. Chem.* 278:15679–15684.

Brown, D. A., and E. London. 1998. Functions of lipid rafts in biological membranes. *Annu. Rev. Cell Dev. Biol.* 14:111–136.

Baumgart, T., S. T. Hess, and W. W. Webb. 2003. Imaging coexisting fluid domains in biomembrane models coupling curvature and line tension. *Nature.* 425:821–824.

Caroni, P. 2001. Actin cytoskeleton regulation through modulation of $PI(4,5)P_2$ rafts. *EMBO J.* 20:4332–4336.

Craig, S. W., and P. Cuatrecasas. 1975. Mobility of cholera toxin receptors on rat lymphocyte membranes. *Proc. Natl. Acad. Sci. USA.* 72:3844–3848.

Dietrich, C., L. A. Bagatolli, Z. N. Volovyk, N. L. Thompson, M. Levi, K. Jacobsen, and E. Gratton. 2001. Lipid rafts reconstituted in model membranes. *Biophys. J.* 80:1417–1428.

Drevot, P., C. Langlet, X. J. Guo, A. M. Bernard, O. Colard, J. P. Chauvin, R. Lasserre, and H. T. He. 2002. TCR signal initiation machinery is preassembled and activated in a subset of membrane rafts. *EMBO J.* 21: 1899–1908.

Edidin, M. 2003. The state of lipid rafts: from model membranes to cells. *Annu. Rev. Biophys. Biomol. Struct.* 32:257–283.

Fahey, P. F., D. E. Koppel, L. S. Barak, D. E. Wolf, E. L. Elson, and W. W. Webb. 1977. Lateral diffusion in planar lipid bilayers. *Science.* 195: 305–306.

Giocondi, M. C., V. Vie, E. Lesniewska, J. P. Goudonnet, and G. Le Grimellec. 2000. In situ imaging of detergent-resistant membranes by atomic force microscopy. *J. Struct. Biol.* 131:38–43.

Ha, T. 2001a. Single-molecule fluorescence methods for the study of nucleic acids. *Curr. Opin. Struct. Biol.* 11:287–292.

Ha, T. 2001b. Single-molecule fluorescence resonance energy transfer. *Methods.* 25:78–86.

Hagmann, J., and P. H. Fishman. 1982. Detergent extraction of cholera toxin and gangliosides from cultured cells and isolated membranes. *Biochim. Biophys. Acta.* 720:181–187.

Hao, M., S. Mukherjee, and F. R. Maxfield. 2001. Cholesterol depletion induces large scale domain segregation in living cell membranes. *Proc. Natl. Acad. Sci. USA.* 98:13072–13077.

Heerklotz, H. 2002. Triton promotes domain formation in lipid raft mixtures. *Biophys. J.* 83:2693–2701.

Kahya, N., D. Scherfeld, K. Bacia, B. Poolman, and P. Schwille. 2003. Probing lipid mobility of raft-exhibiting model membranes by fluorescence correlation spectroscopy. *J. Biol. Chem.* 278:28109–28115.

Kahya, N., D. Scherfeld. K. Bacia, and P. Schwille. K. Scherfeld. K. Bacia, and P. Schwille. 2004. Lipid domain formation and dynamics in giant unilamellar vesicles explored by fluorescence correlation spectroscopy. *J. Struct. Biol.* 147:77–89.

Klausner, R. D., and D. E. Wolf. 1980. Selectivity of fluorescent lipid analogues for lipid domains. *Biochemistry.* 19:6199–6203.

Klein, U., G. Gimpl, and F. Fahrenholz. 1995. Alteration of the myometrial plasma membrane cholesterol content with β-cyclodextrin modulates the binding affinity of the oxytocin receptor. *Biochemistry.* 34:13784–13793.

Korlach, J., P. Schwille, W. W. Webb, and G. W. Feigenson. 1999. Characterization of lipid bilayer phases by confocal microscopy and fluorescence correlation spectroscopy. *Proc. Natl. Acad. Sci. USA.* 96: 8461–8466.

Marsh, D., A. Watts, and P. F. Knowles. 1976. Evidence for phase boundary lipid. Permeability of tempo-choline into dimyristoylphosphatidylcholine vesicles at the phase transition. *Biochemistry.* 15:3570–3578.

Marsh, D., A. Watts, and P. F. Knowles. 1977. Cooperativity of the phase transition in single- and multibilayer lipid vesicles. *Biochim. Biophys. Acta.* 465:500–514.

McConnell, H. M., and M. Vrljic. 2003. Liquid-liquid immiscibility in membranes. *Annu. Rev. Biophys. Biomol. Struct.* 32:469–492.

Munro, S. 2003. Lipid rafts: elusive or illusive? *Cell.* 115:377–388.

Pike, L. J., and J. M. Miller. 1998. Cholesterol depletion delocalizes phosphatidylinositol bisphosphate and inhibits hormone-stimulated phosphatidylinositol turnover. *J. Biol. Chem.* 273:22298–22304.

Pralle, A., P. Keller, E. L. Florin, K. Simons, and J. K. Horber. 2000. Sphingolipid-cholesterol rafts diffuse as small entities in the plasma membrane of mammalian cells. *J. Cell Biol.* 148:997–1008.

Saxton, M. J. 1994. Anomalous diffusion due to obstacles: a Monte Carlo study. *Biophys. J.* 66:394–401.

Schroeder, R., E. London, and D. Brown. 1994. Interactions between saturated acyl-chains confer detergent resistance on lipids and glycosylphosphatidylinositol (GPI)-anchored proteins: GPI-anchored proteins in liposomes and cells show similar behavior. *Proc. Natl. Acad. Sci. USA.* 91:12130–12134.

Schuck, S., M. Honsho, K. Ekroos, A. Shevchenko, and K. Simons. 2003. Resistance of cell membranes to different detergents. *Proc. Natl. Acad. Sci. USA.* 100:5795–5800.

Schütz, G. J., and P. Hinterdorfer. 2002. Single molecule fluorescence and force microscopy. *Exp. Gerontol.* 37:1493–1509.

Schütz, G. J., G. Kada, V. P. Pastushenko, and H. Schindler. 2000. Properties of lipid microdomains in a muscle cell membrane visualized by single molecule microscopy. *EMBO J.* 19:892–901.

Schwille, P., J. Korlach, and W. W. Webb. 1999. Fluorescence correlation spectroscopy with single-molecule sensitivity on cell and model membranes. *Cytometry.* 36:176–182.

Seveau, S., R. J. Eddy, F. R. Maxfield, and L. M. Pierini. 2001. Cytoskeleton-dependent membrane domain segregation during neutrophil polarization. *Mol. Biol. Cell.* 12:3550–3562.

Siggia, E. D., J. Lippincott-Schwartz, and S. Bekiranov. 2000. Diffusion in inhomogeneous media: theory and simulations applied to whole cell photobleach recovery. *Biophys. J.* 79:1761–1770.

Simons, K., and E. Ikonen. 1997. Functional rafts in cell membranes. *Nature.* 387:569–572.

Simons, K., and G. van Meer. 1988. Lipid sorting in epithelial cells. *Biochemistry.* 27:6197–6202.

Spink, C. H., M. D. Yeager, and G. W. Feigenson. 1990. Partitioning behavior of indocarbocyanine probes between coexisting gel and fluid phases in model membranes. *Biochim. Biophys. Acta.* 1023:25–33.

Thomas, J. L., D. Holowka, B. Baird, and W. W. Webb. 1994. Large-scale co-aggregation of fluorescent lipid probes with cell surface proteins. *J. Cell Biol.* 125:795–802.

Thompson, N. L., and D. Axelrod. 1980. Reduced lateral mobility of a fluorescent lipid probe in cholesterol-depleted erythrocyte membrane. *Biochim. Biophys. Acta.* 597:155–165.

Widengren, J., and P. Schwille. 2000. Characterization of photoinduced isomerization and back-isomerization of the cyanine dye cy5 by fluorescence correlation spectroscopy. *J. Phys. Chem. A.* 104:6416–6428.

Yeagle, P. L. 1991. The Structure of Biological Membranes. CRC Press, Boca Raton, FL.

Yoon, S. S., K. I. Jung, Y. L. Choi, E. Y. Choi, I. S. Lee, S. H. Park, and T. J. Kim. 2003. Engagement of CD99 triggers the exocytic transport of ganglioside GM1 and the reorganization of actin cytoskeleton. *FEBS Lett.* 540:217–222.